J. Condensed Matter Nucl. Sci. 39 (2025) 196–209

Research Article

Achieving Very High Incremental LANR Power Gain

Mitchell R. Swartz ScD MD EE
JET Energy, Inc., Wellesley Hills, MA, USA

Abstract

Very high levels of incremental power gain can be achieved from preloaded, dry, active NANOR®-type components. These components are many orders of magnitude greater power, and energy, when compared to ohmic controls, for the same electrical input. These large amounts of power gain pave the way to future commerce and technical improvements.

Keywords: fusion, synchronization, lattice assisted nuclear reaction, incremental power gain

1. Introduction

Thirty-five years of solid sterling evidence heralds that the excess heat ["XSH"] sought and elicited by CF/LANR is very real [1]. The CF/LANR information is always best demonstrated as follows: first an ohmic control at the same input power (and impedance when possible), then the measurement, with inclusion of the integrated energy for both input and output [confer Figure 1], and the background thermal power.

The XSH provided is now known to arise from deuterons as fuel along a nuclear path of fusion [2], [3], [4]. Ultimately, however, what is of major importance is: obtaining large values of the actual, desired product and large values of incremental power gain [output power divided by; the input power]. These large amounts are requisite for both commerce and technical improvements. Theories have less importance. Therefore, the ultimate CF/LANR keys to the future are improved alloy lattices, higher incremental power gains, and the duration that the excess heat can be continued before loss of the active alloy. In the past, we have shown how to successfully obtain, confirm, measure, and utilize excess heat for a number of years, in both aqueous PdD [refs. 5 to 12] and preloaded ZrO2-PdD nanomaterial components and systems [refs. 13 to 27]. This report quantitatively goes far beyond.

2. Background – Dry Preloaded ZrO2-PdNiD NANOR®-type LANR Component

NANOR®-type LANR Components are a new generation of CF/LANR quantum electronic devices exhibiting considerable energy gain. These important, novel devices feature two terminals with a cylindrical shape and active CF/LANR core and self-contained superior handling properties enabling portability and transportability. Most importantly, the activation of the cold fusion/lattice assisted nuclear reaction is, for the first time, separated from loading. These

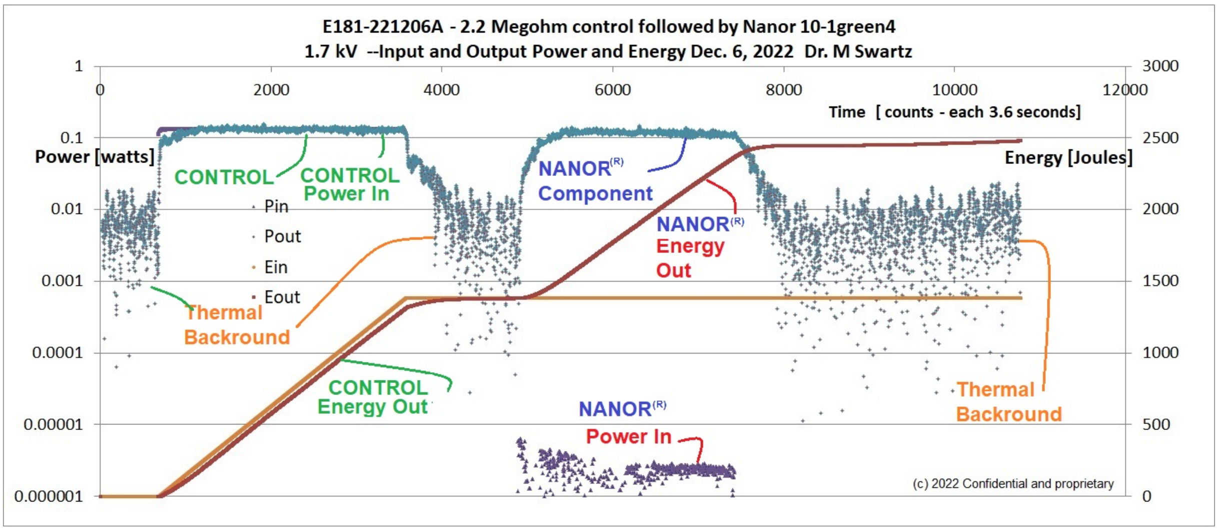

Figure 1. Input and Output Powers and Energies from an Electrically Driven Ohmic Control and then NANOR® N10-1G4, and the Thermal Background. The graph shows the response of NANOR®-type Component N10-1G4, and an ohmic control, in Run E181-221206A. The horizontal axis is time, and here is labeled by counts; with each being 3.6 seconds. The ohmic control was electrically driven prior to the LANR component. The input and output powers are read off the left hand logarithmic values. The energies are read off the right hand axis.

NANOR®-type preloaded components are dry, sealed into an electrically conductive (high impedance) configuration. Thus, they are incredibly useful and have demonstrated a more reproducible CF/LANR behavior.

These dry, preloaded nanocomposite components are about 2 centimeters length, with 30 to 200 milligrams of active LANR material, at an LANR excess power density that is more than 19,500 watts/kilogram of nanostructured material. The small, preloaded, dry components have enabled the way to higher instantaneous power gain, total energy gain, imaging [19], emissions [18], open demonstrations [13], [14], and a better understanding of the impact of applied magnetic fields [15], [21], and electrical transconduction [20]. Most importantly, relevant to their desired function, we have demonstrated that several electrical transconduction states exist, but that only one is active, desired, and capable of producing "excess heat" [12]. The other is non-functional, essentially 'dead', with no production of the desired excess heat.

The NANOR®-type components, such as NANOR #7-24, have a ZrO_2-PdD core with copper or palladium contacts. This Series 7 component has a core of ZrO_2-(PdD) with Zr ($\sim$95%) by weight before the oxidation step, and before the final entry of the deuterons over months. NANOR® N10-1G4 was a gas loaded Series 10 component. NANOR®-type component N14-7 is a Series 14 component, made from Dr. Yoshiaki Arata's base nanomaterial with Wickian loading. JET Energy, Inc. has developed several types of deuteron loading (and measurement); Wickian loading is the most efficient, and fastest, of its proprietary methods.

2.1. Experimental Methods – Electric Power Drive

Precision input power and energy control is done by using either controlled power sources like a Keithley current source, or regulated power supplies (as used for amateur radio) with DAQ, including Arduino and computer controlled power supplies (like Tekpower TP3005P). The Arduino drives a transistor or MOS-FET using PWM. These electrical systems deliver precise current step functions sequentially to either the ohmic control or the NANOR®-type component. Errors are minimized by the boron nitride (insulator) and the other plastics used (PLA from the 3D printing). The excess heat results from electrically driving the ZrO_2PdD preloaded NANOR®-type LANR component [13], [14] carefully below its avalanche voltage [20], [12], above which the excess heat production is known to cease.

There is a role for careful sequencing input power to both the component and the ohmic control. As the figures below demonstrate, each is directly shown, including the electrical input and the thermal ("heat") output as a function of time. Cool off time was allowed between the control and the activated LANR component. Such thermal calibration is always used.

Ohmic controls also are always used. The advantage of using an ohmic control square wave immediately before the CF/LANR run is that one can also simultaneously check – and compare - the performance of your calorimeters' analysis. For each step pulse, the thermal ohmic control and then the component under test are examined by a constant input power. This provides heat at a constant rate from electrical dissipation (V*I) which is maintained over a long period of time (longer than the time response of the core under test). The algorithm converts the thermometry to ohmic control-calibrated calorimetry. Confirmation of the algorithm is made by checking the appearance of the output heat from the ohmic control. If it does not produce the applied square wave then the system is flawed.

We try to closely match the electrical input power to BOTH ohmic control and the NANOR®-type component ["power bracketing"]. Such electrical input power bracketing should be delivered to the LANR component or device under measurement for the "excess power". Finally, the use of energy, obtained through time integration of the power, is actually necessary to also prove one's analytic system is correct, and to rule out phase changes, and the like. That is done here.

In any real setup, the electrical impedance of the NANOR®-type component changes with time, and depends on past history to some degree. This is because the NANOR®-type compound has an electrical impedance that demonstrates hysteresis, and can also undergo an electrical avalanche if the voltage is excessive. Therefore, for that case, we match electrical input power by adjusting voltage as necessary.

In addition, there is actually some time variance of electrical resistivity that occurs for ohmic controls as well, due to use and changing temperature, but that is minimal and second order.

2.2. Experimental Methods - *in situ* Sensors Used

Several types of detection methods were used while electrically driving the system. In addition to our publications, we include custom DS18B20 temperature sensors. Arduino Libraries are required [MAX6675, OneWire (wire.h), and MAX31850 Dallas Temp (DallasTemperature.h)] for each. The forces are determined by accelerometers and gyroscopes. The MPU-6050 has a 3-Axis accelerometer and a 3-Axis gyroscope integrated in situ. These are MEMS sensors with 16-bits analog to digital conversion for each of the 6 channels. These are then output to the I2C-bus.

We measure the vectored acceleration, perform a vectorial RMS addition, and multiply that derived acceleration by the effective mass. We demonstrated that by taking the square of each of the orthogonal vector components and then vectorally adding them, and then taking the square root of the magnitude, this would produce the actual RMS magnitude. This has yielded much improved S/N ratios. The RMS magnitude has been incredibly helpful in both the LANR magnetic field experiments and here in these nitinol vector force measurements. The effective mass includes the component, the temperature sensor, and some fraction of the leads, spring, etc. around all of the components.

2.3. Experimental Methods – Calorimetry

Power calorimetry is determined by analysis of the dynamic changes of temperature measurements at several locations. For good, calibrated measurements, the electrically-driven active components are always timely compared to an ohmic control. They are put into the same volume and wrapped in boron nitride [BN] and a larger thermal mass, along with a thermocouple(or equivalent). BN is a soft blue material, that acts like clay and is thermally conductive and electrically insulating.

This mass ensemble is examined by thermometry before, during, and after electrical drive, and calibrated by the thermal ohmic control. The results are confirmed by long-term time integration. Confirmation of the algorithm, checking for linearity and time-invariance, and calibrating the output of the component under test, is made by reproducing the heat generated from a square wave sent to an ohmic control. Thus, this calibration is important in several ways. Experimentally, the ohmic control is first used and compared to an active NANOR®-type component. In addition to calibrating the calorimeter, it also establishes the baseline by first measuring and observing the response of the ohmic control.

In summary, the experimental setup includes calorimetry, and bracketing of the NANOR®-type component with ohmic controls in time and by input electric power applied, and includes time integration to rule out false positives. Thus, a good comparison can be made to determine if putative incremental excess power is present.

3. Results – Incremental Power Gain can be Significantly Large

As a result of this meticulous effort, we have now found there can be obtained very high levels of incremental power gain [Figures 1 through 9]. Different paradigms were used which demonstrate reproducibility several ways. For example, in Figure 1, the paradigm has the ohmic control matched with respect to input power to the NANOR® type component.

In fact, as shown in Figure 1, the incremental power gain obtained from the preloaded, active NANOR®-type Component N10-1G4 in Run E181-221206A is many orders of magnitude greater when compared to the ohmic control. Note how many orders of magnitude the electrical input to the NANOR®-type component was below the thermal background. Yet even that tiny input has, by LANR, produced very large energies out (logarithmic right axis) far in excess of the input energy. The incremental CF/LANR power gain is about 6 x 10^4. The time constant, when the NANOR was turned on, is about 1500 sec.

The incremental power gain (proportional to the actual excess heat) of CF/LANR is clearly seen, with much better incremental gain than we saw with the PHUSOR®-type D_2O components in 2003 (ICCF-10 open demonstration - with gains to circa 480%), and better than with NANOR®-type ZrO2NiPdD components in 2012 (at the MIT IAP Course, then with a gain of only 12 (1200%), later increased to a gain of $\sim$80 with magnetic fields applied synchronously). Now, this report augments that with the confirmation of very high achievable LANR incremental power gains.

Figure 2 shows the input and output electrical powers, and resultant energies, from an electrically-driven ohmic control resistor, followed by NANOR® N10-1G4. The figure also shows the thermal background power.

In Figure 2, note how many orders of magnitude the electrical input to the NANOR®-type component N10-1G4 was below the thermal background. Yet even that tiny input has, by LANR, produced very large energies out (logarithmic right axis) far in excess of the input energy. The incremental power gain obtained from the preloaded, active NANOR®-type component is many orders of magnitude compared to the ohmic control in Run E181-221130A. The incremental CF/LANR power gain is about 9×10^4.

Figure 3 shows the input electrical power and resultant incremental power gain, if any, for NANOR®-type Component N10-1G4 and an ohmic control, in Run E181-221201A. The normal power gain for the ohmic control is 1.0. By contrast, yet even with a smaller input power, notice that LANR has produced a very large incremental power gain (on that right hand axis). Notice that in Figure 3, the incremental power gain obtained from the preloaded, active NANOR®-type component is many orders of magnitude larger compared to the ohmic control. The difference reflects the excess heat actually achieved in this LANR system.

Figure 4 shows the input electrical power delivered to an ohmic control and then NANOR®-type component N7-24. The Figure also shows the resultant mechanical response of some neighboring Nitinol. Excess power (beyond that

NANOR®-type Component N10-1G4 and an ohmic control in Run E181-221130A

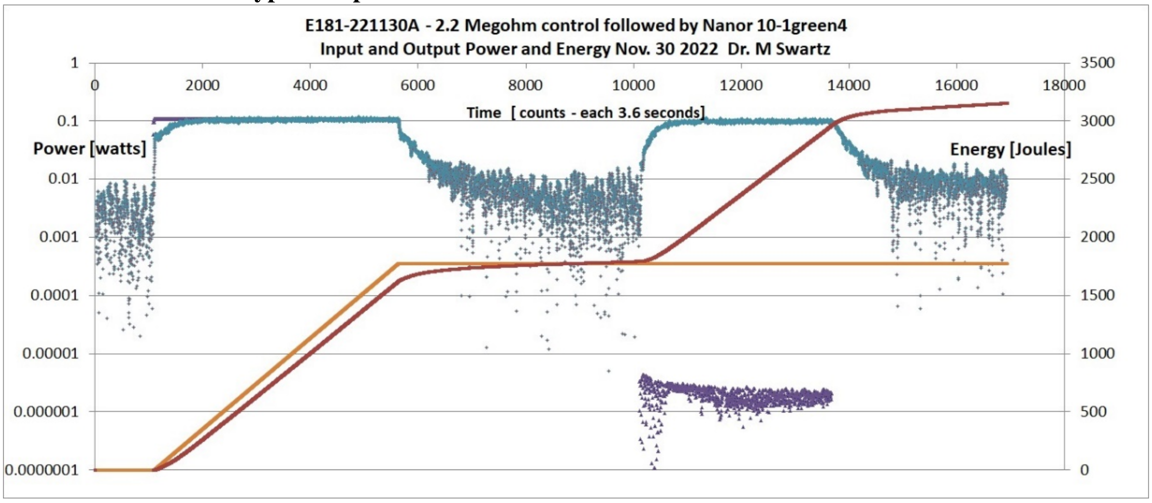

Figure 2. Input and Output Powers and Energies from an Electrically Driven Ohmic Control and then NANOR® N10-1G4, and the Thermal Background. This graph shows the response of NANOR®-type Component N10-1G4, and an ohmic control, in Run E181-221130A. The horizontal axis is time, and here is labeled by counts; with each being 3.6 seconds. The ohmic control was electrically driven prior to the LANR component. The input and output powers are read off the left hand logarithmic values.

NANOR®-type Component N10-1G4 and an ohmic control in Run E181-221201A

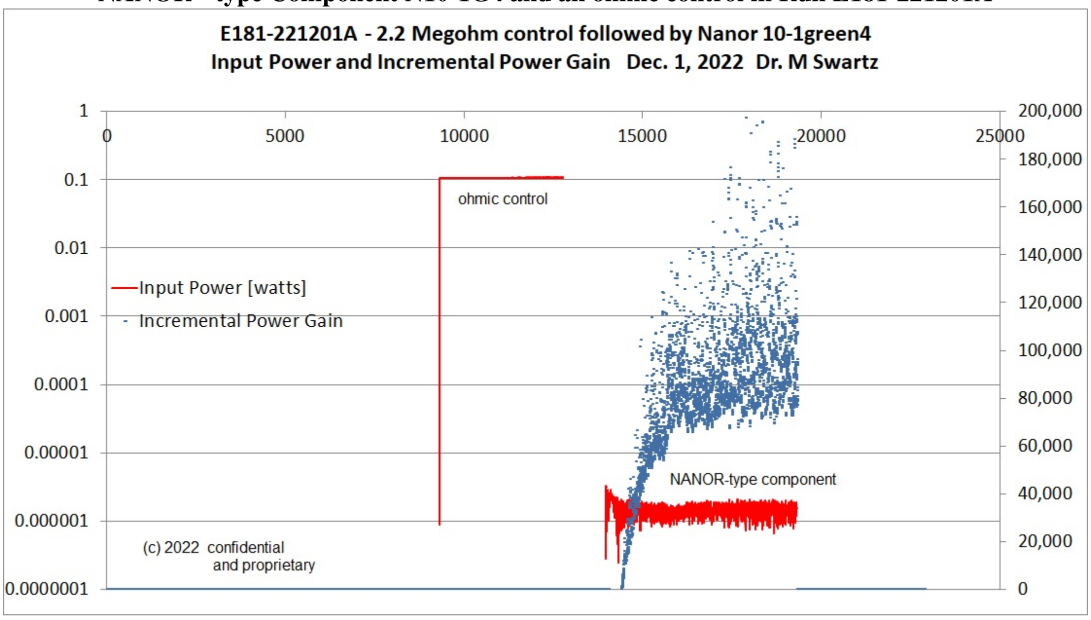

Figure 3. Input Power and Incremental Power Gain for NANOR®-type Component N10-1G4 and an ohmic control in Run E181-221201A. This graph shows the Input Power and Incremental Power Gains in response, for both an ohmic control and NANOR®-type Component N10-1G4 in Run E181-221201A. The horizontal axis is time. The ohmic control was electrically driven prior to the LANR component. The input powers are read off the left hand logarithmic axis, and values.

NANOR®-type Component N7-24 and an ohmic control in Run E127-201009A

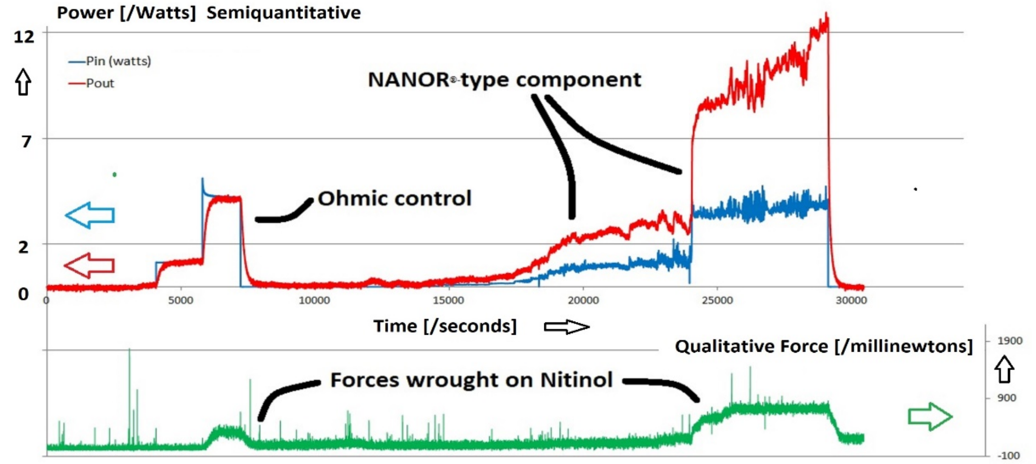

Figure 4. Input Electrical Power delivered to an Electrically Driven Ohmic Control and then NANOR®-type component N7-24 in Run E127-201009A and the Resultant Output Thermal Power and the Mechanical Response on Neighboring Nitinol. Shown is the input (blue) and output (red) electrical power from the Ohmic Control and NANOR® type component Nanor N7-24 as a function of time. Also shown is the Response of neighboring Accelerometer (shown as the RMS force; in green by the lower curve) which is the force wrought by the heat (regular and excess, if present) upon the nitinol.

which was applied) can be easily seen for the preloaded ZrO2-PdD. This demonstrates that there was salient LANR activity by NANOR®-type Component N7-24 in Run E127-201009A. In Figure 4, it can also be seen that one can then measure and discern the differential response between the ohmic control and a NANOR®-type component where both are physically and thermally attached to the nitinol and thermocouple.

Figure 5 shows the applied input voltage and the resultant incremental power gain, if any, for an ohmic control and then NANOR®-type Component N14-7, after it was fully deuteron loaded. Note how many orders of magnitude the incremental power gain increased compared to the control. A massive incremental power gain was obtained from the preloaded, active NANOR®-type component compared to the ohmic control where the power gain was only 1.0.

In Figure 5, notice that the incremental power gain of the NANOR®-type component, even though initially very high, falls even as the input voltage across it increases.

This decrease in incremental power gain, with applying increased voltage, is important.

Figure 6 shows the applied input voltage and the resultant incremental power gain for an ohmic control resistor and the NANOR®-type Component N14-7, after it was fully deuteron loaded.

Note how many orders of magnitude the incremental power gain was when obtained from the preloaded, active NANOR®-type component compared to the ohmic control where the power gain is only 1.0.

Figure 7 shows the elicited delta-T and the calculated incremental power gain for an ohmic control resistor and then NANOR®-type Component N14-7, after it was fully deuteron loaded. Note how many orders of magnitude the incremental power gain from the NANOR®-type component was compared to the ohmic control, where the delta-T is barely noticeable, and the power gain is about 1.0.

Figure 8 shows the histogram of power gain measured for NANOR®-type Component N14-7 during run E549-240321A. The histogram reveals the number of times during the run, that each incremental power gain (listed on the x-axis) was seen. This idea is novel and was suggested by John Wallace.

NANOR®-type Component N14-7 and an ohmic control in Run E549-240320A

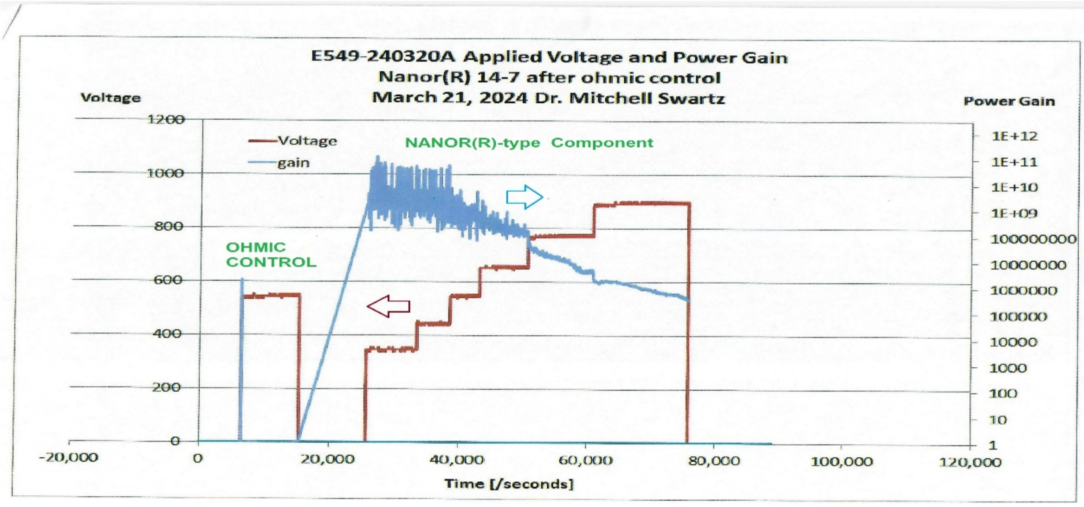

Figure 5. Applied Input Voltage and the Resultant Incremental Power Gain For an Ohmic Control and NANOR®-type Component N14-7 Fully Loaded. This graph shows the response of NANOR®-type Component N14-7, after its previous full deuteron loading, and an ohmic control, in Run E549-240320A. The horizontal axis is labeled in seconds. The ohmic control was driven prior to the LANR preloaded component. The applied input voltage and the calculated effective incremental power gain of both the ohmic control and the LANR component are read off the left hand voltage axis and the right hand logarithmic incremental power gain axis, respectively.

NANOR®-type Component N14-7, and an ohmic control, in Run E549-240323A

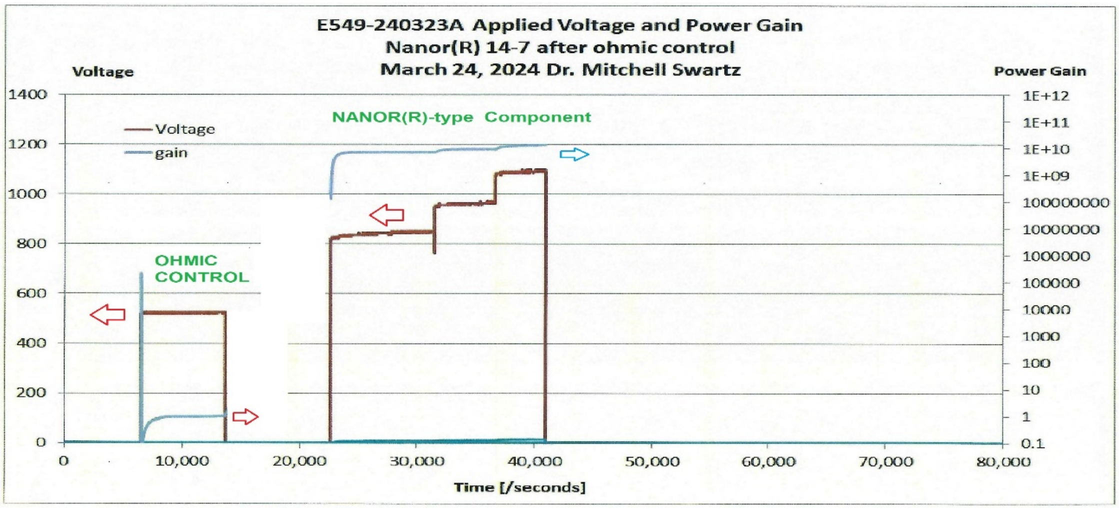

Figure 6. Applied Input Voltage and the Incremental Power Gain For an Ohmic Control and NANOR®-type Component N14-7 Fully Loaded. This graph shows the response of NANOR®-type Component N14-7, and an ohmic control, in Run E549-240323A. The horizontal axis is labeled in seconds. The ohmic control was driven prior to the LANR preloaded component. The applied input voltage and the calculated effective incremental power gain of both are read off the left hand voltage axis and the right hand logarithmic incremental power gain axis, respectively.

NANOR®-type Component N14-7, and an ohmic control, in Run E549-240324A

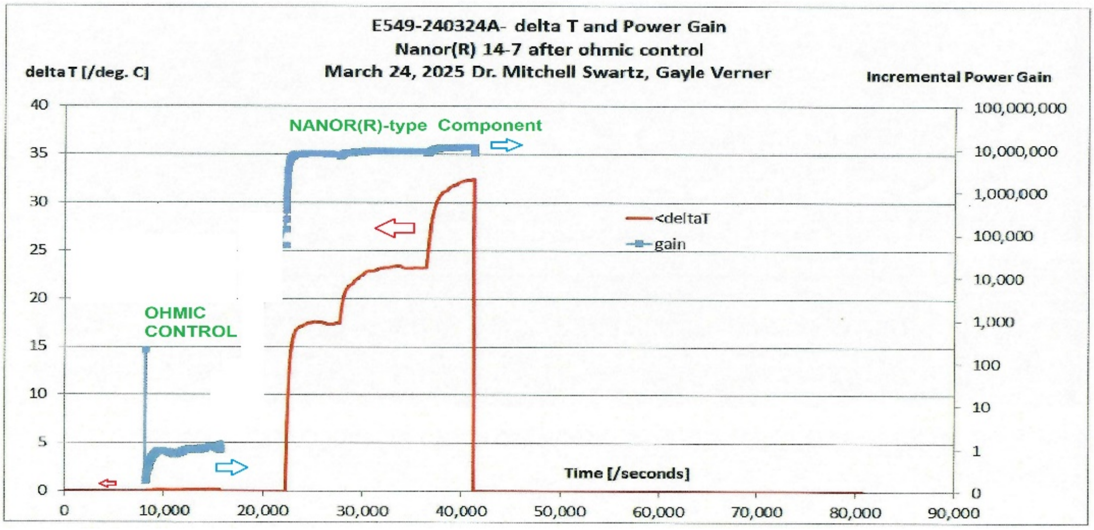

Figure 7. Elicited delta-T and the Incremental Power Gain For an Ohmic Control and NANOR®-type Component N14-7 Fully Loaded. This graph shows the response of NANOR®-type Component N14-7, and an ohmic control, in Run E549-240324A. The horizontal axis is labeled in seconds. The ohmic control was driven prior to the LANR preloaded component. The induced delta-T and calculated effective incremental power gain of both the ohmic control and the LANR component are read off the left hand temperature axis and the right hand logarithmic incremental power gain axis, respectively.

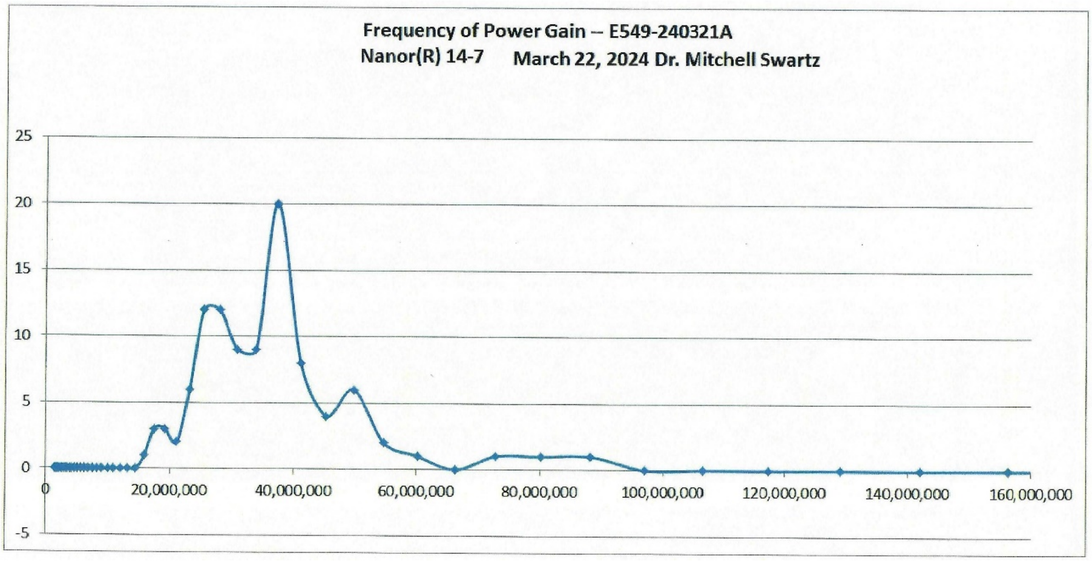

Figure 8. Frequency of Power Gain for NANOR®-type Component N14-7 During Run E549-240321A. The graph is a histogram of the results during Run E549-240321A. The histogram shows the Frequency of Power Gain results which were obtained from NANOR®-type Component N14-7 during that run. It reveals the number of times during the run, that each incremental power gain (listed on the x-axis) was seen.

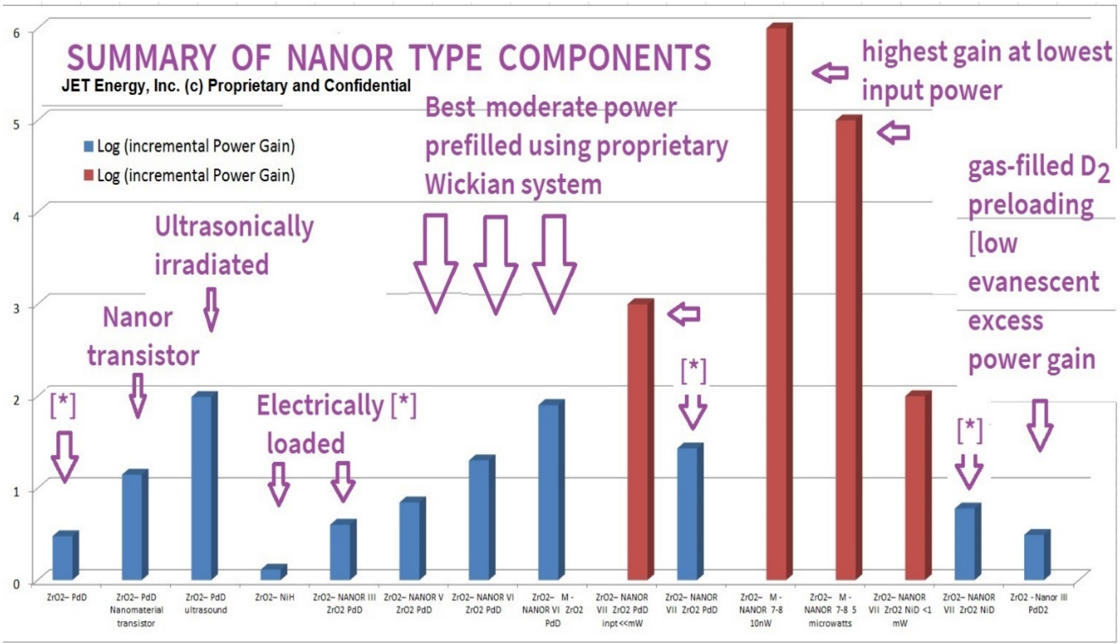

Figure 9. Summary of Incremental Power Gain For Thousands of LANR Experiments. This graph of Incremental Power Gain (on a Logarithmic vertical axis) shows the results of thousands of LANR experiments of three decades. Loading by gas, or by electrochemisty, or Wickian technology have been used successfully.

In summary, these findings of achievable high incremental power gain continue increasing. Improved loading of deuterons, and improved avoiding of electric avalanche have helped the most. The results are shown in Figure 9 and Figures 1 through 7. The highest peaks are truly the energy production roads 'less traveled' in this field.

The incremental power gains are read off the right hand axis.

4. Non-Confrontational Fusion [LANR] Works

4.1. Interpretation - Loaded Deuterons Interact Synchronously in LANR

LANR works because of Bose synchronous interactions between the deuterons in highly loaded palladium. Their interaction is revealed by anti-Stokes measurements, and radio frequency (RF) emissions when they result in WORKING CF/LANR systems and components.

This occurs for both aqueous PdD [refs. 5 to 12] and preloaded ZrO2-PdD nanomaterial components and systems [refs. 13 to 27]. The loaded deuterons interact through Band States (S. Chubb, and T. Chubb, and Kim) and other interactions (Bass, and others), and through optical interactions which provide activation energies (and more; Cravens, Letts, Swartz). In successful LANR, the pathway to deuteron fusion is first initiated by electrically-forced turbulent oscillator flow. Then, with full loading, pairs (or probably more) of loaded deuterons located in periodic vacancies, in the highly loaded lattice, interact synchronously producing dynamic interactions.

These now-coupled ionized deuterons are identical boson oscillators and interchange amongst themselves without any change in the system. This is a permutation symmetry called Z_2 ["Huygens (clock) symmetry"].

5. Interpretation – An Excited 4He* State is Obtained in LANR

The successful CF/LANR condensed matter reactions of Pd/D_2O/Pt which form *de novo* ^{4}He, first involve an energy gap of between 20 MeV and 24 MeV from the ground state. This megavoltage energy difference is not "low energy", and is capable under some conditions of generating penetrating ionizing radiation, and is sufficient even to incur pair production. CF/LANR is high energy. Phonons (acoustic and optical) enable the transfer of energy from ^{4}He*to the lattice [28], [28]. Therefore, this energy transfer appears as "excess heat", and yields ground state *de novo* ^{4}He.

The excess heat results from the applied electric field which appears to most control the LANR reaction rate. In successful LANR, deuteron synchronization is driven by the applied electric field intensity into electrically-forced turbulent oscillator flow. From this, pairs of loaded deuterons -located in periodic vacancy sites- combine synchronously. Unlike hot fusion, this LANR result is relational and productive. Thus, here, rather than one D hitting the other as a target, there is no conventional "coulomb barrier", but instead synchronous interaction(s) follow.

With cold fusion, 3*10 ** −4 Grays are produced at 1 meter for 1 coulomb. By contrast, in hot fusion, one D hits the other as a target. This is brute targeting, and therefore both confrontational and destructive. The synchronous interaction CAN occur making the lattice able to surmount, circumvent and make moot the previous coulomb barrier. Thus, there is the conventional "coulomb barrier" and 3*10**19 Grays are produced at 1 meter for 1 coulomb.

Vacancies in palladium are the key. A high concentration of deuteron-loaded vacancies enables Bose-enabled deuteron synchronization and their fusion releasing the excess heat from potentially active LANR samples. In successful LANR, the number, and type, and distribution, of vacancies in the Pd and ZrO2 have been discussed elsewhere [25], [27]. The number of vacancies increases after loading over a period of weeks. This results because loading with hydrogen (or deuterons) slightly decreases the energy required to make each one. Most interesting, as the radiofrequency [RF] emission sidebands demonstrate, a very small number of the types of vacancies apparently change slightly when the excess heat from active samples is wrought [25].

6. Interpretation – AntiStokes Peaks Herald Acoustic Phonons in LANR

Dual wavelength coherent-enhanced electric-driven reflection spectroscopy revealed the unique antiStokes signatures which ONLY appear with active LANR systems during excess heat ["XSH"] production. This method can illuminate the important optical differences between the well-known two (2) driven LANR states, but of which only one (1) gives excess heat.

The revealed antiStokes LANR-wrought peaks in addition herald, and prove, one important role for phonons in successful CF/LANR. Previously, cold fusion investigators had not been able to directly see phonons in their hydrogen loaded systems, although the different material/metallurgical states had been inferred indirectly through beat-frequency two-wavelength systems, and thought to be mainly optical phonons.

Prof. Peter Hagelstein first incorporated optical phonons in his theory decades ago. However, this new diagnostic enables direct visualization of the actual phonon states, even while the device/system is electrically driven. Specifically, we have now observed that PdD acoustic phonons result from, and are possibly required for, successful CF/LANR. The coherent anti-Stokes spectroscopy CF/LANR studies herald that acoustic phonons also have an indelible role and are involved in the excess heat for active cold fusion (LANR) systems. The coherent Raman spectroscopy can be used to provide the data of the fusion. The Stokes and anti-Stokes energies are quite derivable, and therefore the calculated number of phonons involved during excess heat can be computed, as follows. As discussed in solid state texts [31], [25], [26], with an acoustic frequency of 4.9 $^{+/-0.1}$ terahertz, there are $\sim$7 $^{+/-0.15}$ acoustic phonons involved.

The number 7 may seem arbitrary until we consider physical relative matters. The vacancy is surrounded by six deuterons plus a central body in the vacancy, totaling 7 [22], [23], [24]. The deuterons move in acoustic mode unison in synchrony to form He4, releasing 24 MeV of energy with each reaction. This augmented theory explains the massive energy cooperative transfer from the megavoltage energy of the ^{4}He* to the lattice in a coherent de-excitation process which proceeds by way of acoustic phonons, lossy-spin optical phonons [28], [29], and possibly magnons [15].

Why is the anti-Stokes/Stokes ratio so high when there is the excess heat (XSH) mode in ZrO_2PdD and in aqueous systems such as the MOAC? That Boltzmann Stokes ratio is significant evidence of acoustic phonon gain, which itself is present only while the preloaded NANOR-type component is electrically driven. The highest levels indicate that the active CF/LANR system occurred, and that has been confirmed by the CMORE-spectroscopy, when the component was driven properly.

How does the desired excess heat mode actually create the anti-Stokes spectra at levels higher than that observed for all other material precursors and avalanche modes?

The fact that the Boltzmann Stokes ratio is $\sim$1.3 reveals either the requisite ratio, or the output ratio of, successful cold fusion. Most importantly, that ratio is far outside of the range expected normally by temperature alone. It is a level greater than could be accounted for by a prosaic curve shift secondary to temperature. The ratio is in a region which is beyond any known calculated temperature.

What are the implications of an XSH-related anti-Stokes to Stokes (aS/S) ratio greater than one?

First, comes cold fusion.

Second, comes a better understanding of the desired cold fusion/LANR XSH state. With LANR success, only *de novo* and relatively low-momentum helium nuclei are formed. This is how.

6.1. Interpretation – Fusion Temperature in LANR is Measureable

However, because both the Stokes- and antiStokes-energies are derivable, the effective Stokes temperature can be computed from the experimental data to reveal the core temperature during the excess heat mode. The next equation derives the calculated Boltzmann Stokes Ratio and the calculated Boltzmann Statistic ratio. The equation involves temperature, and is

$R_{aS/S(calculated)} =$ Intensity(anti-Stokes)/Intensity(Stokes) = exp $(-E_{diff}/(k_B{*}T))$

where E_{diff} is the energy difference between the two states is 5.96 10^{-21} J and k_B is Boltzmann's constant. The solution implies that the calculated temperature at core is, therefore, $\sim$1645 degrees Kelvin ($\sim$1372 Centigrade).

6.2. Interpretation – Deuterons Interact Producing High-Q RF Emissions

Active electrically-driven LANR systems, both aqueous and dry preloaded nanomaterial, emit a hyperfine radiofrequency (RF) maser emission $\sim$327.37 MHz, near the theoretical Deuteron-Line (DL; 327.348 MHz). The LANR maser exhibits a very large Q > 1.2×10^6 , and a positive Zeeman effect. The LANR active state's RF emission, at the Deuterium line, also creates a new method to observe LANR systems.

New information about LANR's difficult-to-attain most-desired XSH mode was discovered at higher applied voltages which reveal superhyperfine sidebands.

Perhaps most importantly, the D-line emission frequency confirms the role of deuterium in LANR [25], [26], [27]. Even more remarkably, some of the SHF lines have pulsations with a period of several minutes. Their appearance is unlike everything else examined over the last six years from Earth or galactic origin. It is ONLY associated with an active XSH-producing CF/LANR system. The pulsatile behavior heralds deuteron synchronization.

6.3. Interpretation – Produced XSH Makes Phuson Theory Corroborated

The PHUSON is the quantum particle of coherent energy transfer that appears as 'excess heat' [28], [29]. The process it enables is consistent with conventional physics, at it coherently couples the megavoltage energy of the synchronously-generated ^{4}He* to the lattice. The ^{4}He* returns to the 4He ground state by the toroidal breathing mode [TBM] solution.

This final critical IRREVERSIBLE (because it is >20 MeV) transition occurs coherently by the PHUSON energy transfer, enabled by lossy spin bosons processes through optical phonons (Hagelstein), acoustic phonons (Swartz) and magnons (Swartz). This is what causes and enables the observed excess heat. The result is fusion and loss of two deuterons, with production of *de novo* helium-4, and the generation of massive amounts of the observed excess heat.

During the return to the 4He ground state, the successful CF/LANR fusion is characterized by a well-defined radio frequency emission at the RF Deuterium-line. This is a high-Q RF maser and therefore requires both a tight range of frequency and absence of noise, and heralds, or perhaps enables, the final deuteron synchronization leading to their fusion.

6.4. Interpretation – Neutron, Gamma and Bremsstrahlung Emissions NOT Observed with LANR

The PHUSON theory explains transfer of the nuclear energy ["excess heat"] to the lattice. Physics also explains why there is a great absence of neutron and gamma ray emissions in CF (LANR). The gamma emission branch from the excited state of $^4He^*$ is actually spin-forbidden for both hot and cold fusion [28], [29]. However, at higher hot fusion temperatures the restriction is lifted.

Hot fusion has large activation energies available (it is 'hot'). LANR/CF does not. This absence of adequate activation energy decisively means that that the branch is NOT available, as it is for hot fusion. The only nuclear branches available are those whose band gaps are surmountable by the available activation energy (limited by the ambient temperature and incident radiation).

Most importantly, the emission of neutrons is energy forbidden. This occurs because the neutron emission band is energetically located $\sim$1 MeV above energy level of $^4He^*$. The large energy, compared to k_B*T, makes neutron emission not really allowed, since k_B*T is 1/25 eV ["room temperature"] [28], [29], [30].

Also connected to the temperature is material's Bremsstrahlung emissions. Normally important Bremsstrahlung emissions are not seen with CF/LANR. This is because bremsstrahlung is very temperature-dependent, decreasing by 18 orders of magnitude, becoming absolutely negligible when considered at low (cold fusion, ie room) temperature [30].

7. Conclusion – Very Large Incremental Power Gain Offers Opportunity

Excess heat ["XSH"] elicited by CF/LANR is achievable, including obtaining large values of the incremental power gain [output power divided by the input power]. The NANOR® type components produce many orders of magnitude greater energy, when compared to ohmic controls, for the same electrical input.

Meticulous effort over more than three decades has obtained very high levels of incremental power gains more than 10^4 to 10^6. The incremental power gains were obtained from the preloaded, active NANOR®-type components, and were calibrated by ohmic controls where the power gain is circa 1.0.

The secret of LANR/CF is: 1 microwatt in, 10 watts out, as shown above. Dry preloaded LANR NANOR®-type components, bundled in groups, will make energy production clean.

These incremental power gains are clearly much better than we saw with the PHUSOR®-type D_2O components in 2003 (gains circa 480%), and with NANOR®-type ZrO2NiPdD components in 2012 (gain of $\sim$80 with magnetic fields). This report augments those previous gains with new very high very-achievable LANR incremental power gains. Again, we observed decreases in incremental power gain, with increased applied voltage. Controlling this is very important.

For the first time, we report a histogram of power gains measured for NANOR®-type Component N14-7 during run E549-240321A. These large amounts of power gain, and output powers, enable future commerce and technical improvements. Achieving high incremental power gains has required improved loading of deuterons, and improved avoiding of electric avalanches.

The ultimate CF/LANR keys toward the future require improved alloy lattices, higher incremental power gains, coupling of these components, and extending even further the duration that these excess heat production cycles can be continued.

Acknowledgments

The author acknowledges, and thanks, helpful comments, editorial assistance, ideas, suggestions, and much support from Gayle Verner, Alex Frank, Thomas Farina, Raymond Kurwzeil, Aaron Kleiner, Joshua Gyllinsky, Michael Staker, John Wallace, Andrew Meulenberg, Brian Josephson, Isidor Straus, Peter Hagelstein, Florian Metzler, Dennis Cravens, Jean-Paul Biberian, David Nagel, Dennis Letts, Frank Gordon, Pamela Mosier-Boss, Lawrence Forsley, Louis DeChiaro, Brian Ahern, Jeff Driscoll, Christy Frazier, Win Cuthbert and Carl Page.

This effort was supported by JET Energy Inc. NANOR® and PHUSOR® are registered trademarks. The technology described here is protected by patents pending.

References

[1] Swartz, M., "Survey of the Observed Excess Energy and Emissions In Lattice Assisted Nuclear Reactions", Journal of Scientific Exploration, 23, 4, 419–436 (2009).
[2] Swartz, M. R., Brian Ahern, Charles Haldemann and Alan Weinberg, Excess Heat is Linked to Deuterium Loss in an Aqueous Nickel LANR System, Proc. ICCF-21, Fort Collins, Co.6/3/18 (2018), J. Condensed Matter Nucl. Sci, Vol. 29, 169 (2019)
[3] Swartz, M. R., Synchronization of Vacancy-Loaded Deuterons Enables Successful LANR Mass-Energy Transfer, JCMNS, Proceedings of ICCF24, Vol. 38, 147 (May 2024).
[4] Swartz, M. R., Deuteron Momentum and the Umweg Factor Initiate and Limit Successful CF/LANR, JCMNS, Proceedings of ICCF24, Vol. 38, 161 (May 2024).
[5] Swartz M., Verner G., The Phusor®-type LANR Cathode is a Metamaterial Creating Deuteron Flux for Excess Power Gain, Proc. ICCF14, 2, (2008), p. 458; Ed D.J. Nagel and M.E.Melich, ISBN: 978-0-578-06694-3, 458, (2010).
[6] Swartz M., Excess Power Gain using High Impedance and Codepositional LANR Devices Monitored by Calorimetry, Heat Flow, and Paired Stirling Engines, Proc. ICCF14 1, (2008), p. 123; Ed D.J. Nagel and M.E.Melich, ISBN: 978-0-578-06694-3, 123, (2010).
[7] Swartz, M.R., "Excess Heat and Electrical Characteristics of Type "B" Anode-Plate High Impedance Phusor-type LANR Devices", American Chemical Society, Salt Lake City, UT, Journal of Scientific Exploration, 23, 4, 491–495 (2009).
[8] Swartz, M., G. Verner, "Excess Heat from Low Electrical Conductivity Heavy Water Spiral-Wound Pd/D2O/Pt and Pd/D2O-PdCl2/Pt Devices", Condensed Matter Nuclear Science, Proceedings of ICCF-10, eds. Peter L. Hagelstein, Scott, R. Chubb, World Scientific Publishing, NJ, ISBN 981-256-564-6, 29–44; 45–54 (2006).
[9] Swartz, M., "Can a Pd/D2O/Pt Device be Made Portable to Demonstrate the Optimal Operating Point?", Condensed Matter Nuclear Science, Proceedings of ICCF-10, eds. Peter L. Hagelstein, Scott, R. Chubb, World Scientific Publishing, NJ, ISBN 981-256-564-6, 29–44; 45–54 (2006).
[10] Swartz, M., "Photoinduced Excess Heat from Laser-Irradiated Electrically-Polarized Palladium Cathodes in D_2O", Condensed Matter Nuclear Science, Proc. ICCF-10, eds. Peter L. Hagelstein, Scott Chubb, NJ, ISBN 981-256-564-6, 213–226 (2006).
[11] Swartz, M., G. Verner, "Dual Ohmic Controls Improve Understanding of 'Heat after Death'", Transactions American Nuclear Society, vol. 93, ISSN:0003-018X, 891–892 (2005).
[12] Swartz, M. R, Aqueous and Nanostructured CF/LANR Systems Each have Two Electrically Driven Modes, Proc. ICCF-21, Fort Collins, Co.6/3/18 (2018), J. Condensed Matter Nucl. Sci, Vol. 29, 177 (2019).
[13] Swartz M. R., Verner G., Tolleson, J, Energy Gain From Preloaded ZrO_2–PdNi–D Nanostructured CF/LANR Quantum Electronic Components, J. Condensed Matter Nucl. Sci. 13, 528, (2014).
[14] Swartz M. R., Hagelstein P.I., Demonstration of Energy Gain from a Preloaded ZrO_2–PdD Nanostructured CF/LANR Quantum Electronic Device at MIT, *J. Condensed Matter Nucl. Sci.* 13, 516, (2014).

[15] Swartz M., Verner, G., *et al*., Amplification and Restoration of Energy Gain Using Fractionated Magnetic Fields on ZrO2–PdD Nanostructured Components, *J. Condensed Matter Nucl. Sci.* 15, (2015), p. 66.

[16] Swartz, M. R, Comparison of NANOR-type LANR Components to 238Pu as a Heat Source for Space Flight, J. Condensed Matter Nucl. Sci, Vol. 29, 238 (2019).

[17] Swartz, M. R, Nitinol Can Detect CF/LANR Excess Heat Activity, Proc. ICCF-23, J. Condensed Matter Nucl. Sci., Volume , pages (2022).

[18] Swartz M. R., Incremental High Energy Emission from a ZrO2–PdD Nanostructured Quantum Electronic Component CF/LANR, J. Condensed Matter Nucl. Sci. 15, 92 (2015).

[19] Swartz M.R., Verner, G., et al., Imaging of an Active NANOR®-type LANR Component using CR-39, J. Condensed Matter Nucl. Sci. 15, p. 81 (2015).

[20] Swartz, M.R. P. Hagelstein, G. Verner, Impact of Electrical Avalanche Through a ZrO2-NiD Nanostructured CF/LANR Component on its Incremental Excess Power Gain", ICCF-19, JCMNS, 19, (2016).

[21] MagneticSwartz, M. R, "Oscillating Excess Power Gain and Coerced Magnetic Domains in M-NANOR-type CF/LANR Components", J. Condensed Matter Nucl. Sci. 22, 35–46 (2017).

[22] Swartz, M. R., Hagelstein, P.L., Increased PdD anti-Stokes Peaks are Correlated with Excess Heat Mode, J. Condensed Matter Nucl. Sci. 24, 130–145 (2017).

[23] Swartz, M. R, Increase of an Anti-Stokes Peak at the Cathode of an Electrically-Driven, Active Aqueous Nickel/H_2O/Pt System, J. Cond Matter Nucl. Sci., Vol. 27, 22–29 (2018).

[24] Swartz, M.R. "Optical Detection of Phonon Gain Distinguishes an Active Cold Fusion/LANR Component", JCMNS, 20, 29–53 (2016).

[25] Swartz, M. R, FCC Vacancies in ZrO2PdD RF are the Active LANR Site, Proc. ICCF-22, J. Cond.Matter Nucl. Sci., Volume 33, pages 126–144 (2020).

[26] Swartz, M. R, Active LANR Systems Emit a 327.37 MHz Maser Line, Proc. ICCF-22, J. Condensed Matter Nucl. Sci., Volume 33, pages 80–110 (2020).

[27] Swartz, M. R, Pulsatile Superhyperfine Lines at 327.37 MHz Herald LANR Activity and Possible Mass-Energy Transfer, Proc. ICCF-22, J. Condensed Matter Nucl. Sci. , Volume 33, pages 111-125 (2020).

[28] Swartz, M., "Phusons in Nuclear Reactions in Solids", Fusion Technology, 31, 228–236 (March 1997)].

[29] Swartz, M. R, Quasiparticles, Collective Excitations and Higher-Order Collective Quasi-Excitations in Lattice Assisted Nuclear Reactions, J. Condensed Matter Nucl. Sci. with Excess Heat Mode, J. Condensed Matter Nucl. Sci. 24, 130–145 (2017)

[30] Swartz, M, G. Verner, "Bremsstrahlung in Hot and Cold Fusion", *J New Energy*, 3, 4, 90–101 (1999)].

[31] Christman, J. Richard, Fundamentals of Solid-State Physics, Chaps 6 and 8, Wiley, New York (1988); https://archive.org/details/fundamentalsofso0000chri